

# Phase Transitions during Formation of Ag Nanoparticles on In<sub>2</sub>S<sub>3</sub> Precursor Layers

*Yang Liu\**, Yanpeng Fu, Thomas Dittrich, Rodrigo Sáez-Araoz, Martina Schmid, Volker Hinrichs, Martha Ch. Lux-Steiner, Christian-Herbert Fischer

Helmholtz Center Berlin for Materials and Energy, Hahn-Meitner-Platz 1, D-14109 Berlin, Germany

## **Corresponding Author**

\*E-Mail: [yang.liu@helmholtz-berlin.de](mailto:yang.liu@helmholtz-berlin.de)

**ABSTRACT:** Phase transitions have been investigated for silver deposition onto In<sub>2</sub>S<sub>3</sub> precursor layers by spray chemical vapor deposition from a trimethylphosphine (hexafluoroacetylacetonato) silver (Ag(hfacac)(PMe<sub>3</sub>)) solution. The formation of Ag nanoparticles (Ag NPs) on top of the semiconductor layer set on concomitant with the formation of AgIn<sub>5</sub>S<sub>8</sub>. The increase of the diameter of Ag NPs was accompanied by the evolution of orthorhombic AgInS<sub>2</sub>. The formation of Ag<sub>2</sub>S at the interface between Ag NPs and the semiconductor layer was observed. Surface photovoltage spectroscopy indicated charge separation and electronic transitions in the ranges of corresponding band gaps. The phase transition approach is aimed to be applied for the formation of plasmonic nanostructures on top of extremely thin semiconducting layers.

**Keywords:** In<sub>2</sub>S<sub>3</sub>, Ag nanoparticles, surface photovoltage spectroscopy, phase transitions, ILGAR, LA-ICP-MS

## 1. Introduction

In the past few years, the field of plasmonics for materials and device research has witnessed an explosive growth [1-3]. The integration of plasmonic structures into photovoltaic devices brings up promising applications. Plasmonic light trapping opens the opportunity for enhancing absorption near the band gap and for further reducing the absorber thickness [4]. Silver nanoparticles (Ag NPs) show pronounced plasmonic effects which have been applied, for example, for absorption enhancement in silicon thin-film [5-8] or organic solar cells [9] and which are of great interest for ultra-thin chalcopyrite solar cells [10, 11]. However, the integration of Ag NPs especially into solar cells with chalcopyrite or sulfide absorbers remains challenging, for example, due to dissolving of silver in the matrix [10]. On the other side, plasmonic nanoparticles would be very useful for absorption enhancement in solar cells with extremely thin absorber (local absorber thickness tens of nm) since the folding of the internal surface and therefore the diode saturation current density could be strongly reduced [12, 13]. The idea of this work is based on the creation of stable Ag NPs on top of a semiconducting sulfide absorber which is almost saturated by silver. A related absorber can be, for example,  $\text{Ag}_2\text{S}$  (band gap  $E_g(\text{Ag}_2\text{S}) = 0.9\text{...}1.1$  eV [14, 15]) or  $\text{AgInS}_2$  (band gap  $E_g(\text{AgInS}_2) = 1.96$  for the orthorhombic phase and 1.86 or 2.01 eV for the chalcopyrite phase [16-18]).

The potential of extremely thin  $\text{In}_2\text{S}_3\text{:Cu}$  absorber layers has been demonstrated whereby Cu was diffused from a CuSCN source forming the hole conducting contact [13, 19, 20]. Hence, similar layers with the displacement of Cu by silver are also expected to show potential as extremely thin absorbers. In this work, an  $\text{In}_2\text{S}_3$  precursor layer is used as well but for forming Ag NPs on an extremely thin semiconducting layer based on Ag, In and S. Such extremely thin absorber with Ag NPs can be applied in a solar cell with the structure: Glass/TCO contact/metal oxide/extremely thin absorber with Ag NPs/hole conductor/metal

contact [13]. Advantages of extremely thin  $\text{In}_2\text{S}_3$  precursor layers are (i) that they can be deposited by the spray ion layer gas reaction (spray-ILGAR<sup>®</sup> [21, 22]) technique onto practically any surface and (ii) that silver can be easily incorporated by diffusion from a sprayed trimethylphosphine (hexafluoroacetylacetonato) silver ( $\text{Ag}(\text{hfacac})(\text{PMe}_3)$ ) ethanol solution.

In this work, the amount of silver deposited onto  $\text{In}_2\text{S}_3$  precursor layers was changed systematically in order to study the incorporation of silver, phase transitions (The phrase “phase transition” in this work refers to the variation of compounds in the precursor layer during the deposition of Ag on top.) before reaching saturation of silver in the reacted layer and the formation and growth of Ag NPs on top of a semiconducting layer. For this purpose, the morphology, the silver to indium ratio, crystalline phases, semiconducting properties in terms of transitions energies in relation to charge separation and optical absorption of treated layers were investigated by scanning electron microscopy (SEM), energy-dispersive X-ray emission (EDX), laser ablation inductively coupled plasma mass spectrometry (LA-ICP-MS), X-ray diffraction (XRD), modulated surface photovoltage (SPV) spectroscopy and UV-Vis spectroscopy. A scheme has been deduced for phase transitions towards the formation of Ag NPs on top of an  $\text{AgInS}_2/\text{AgIn}_5\text{S}_8$  compound layer with an  $\text{Ag}_2\text{S}$  interfacial layer.

## 2. Experimental details

$\text{In}_2\text{S}_3$  precursor layers were deposited onto c-Si, glass and molybdenum (Mo)-coated glass substrates by using the ILGAR (ion layer gas reaction) technique [21, 22]. For  $\text{In}_2\text{S}_3$  deposition by ILGAR, a 25 mM precursor solution of indium acetylacetonate ( $\text{In}(\text{acac})_3$ ) dissolved in ethanol was subsequently sprayed onto the substrate and sulfurized in  $\text{H}_2\text{S}$  at 225 °C (14 spray-sulfurization cycles corresponded to an effective layer thickness of  $\text{In}_2\text{S}_3$  of about 90 nm).

Silver was deposited onto  $\text{In}_2\text{S}_3$  precursor layers by spray chemical vapor deposition (spray-CVD) of a  $\text{Ag}(\text{hfacac})(\text{PMe}_3)$  (trimethylphosphine (hexafluoroacetylacetonato) silver) solution. The concentration of  $\text{Ag}(\text{hfacac})(\text{PMe}_3)$  was 10 mM in ethanol. The  $\text{Ag}(\text{hfacac})(\text{PMe}_3)$  solution was nebulized to form an aerosol which was carried by nitrogen gas to the substrate. During the silver deposition, the nitrogen flow rate was 5 liters per minute and the substrate temperature was 200 °C. The silver deposition time was adjusted between 0.17 and 32 min in order to vary the silver content of the samples over a wide range.

The sample morphology was studied by SEM using a field emission gun microscope with an in-lens detector. Maps of the distributed elements (Ag, In and S) were obtained by EDX analysis of the Ag-L, In-L and S-K signals. Both SEM and EDX analysis were performed on a LEO GEMINI 1530 scanning electron microscope equipped with a Thermo Noran X-ray detector. The acceleration voltages applied were 5 kV (SEM) and 10 kV (EDX).

The crystal phases of the samples were studied by XRD with a Bruker D8 X-ray diffractometer operated in the detector scan mode (scanning angle from 10° to 70°) with radiation of a  $\text{Cu K}\alpha$  source (wavelength 0.154056 nm). Crystalline silicon and glass substrates were used for the SEM and XRD investigation, respectively.

The overall molar ratio between Ag and Indium was obtained by LA-ICP-MS for layers deposited on c-Si substrates. For each sample, laser ablation was performed in one line scan with sufficiently high laser power to reach the c-Si surface (CETAC LSX213 laser system, 213 nm laser light frequency, 4 mJ/pulse, 20 Hz pulse frequency, spot size 200  $\mu\text{m}$ , 200  $\mu\text{m}/\text{s}$  scan speed). The Ag/In ratio was calibrated using a reference material (NIST612, containing 23 ppm Ag and 38 ppm In) [23]. The indium signal was constant for all samples within a standard deviation of about 2.4%, indicating a layer of  $\text{In}_2\text{S}_3$  with homogeneous thickness.

Charge separation and electronic transitions were investigated by SPV in the fixed capacitor arrangement [24]. A halogen lamp with a quartz prism monochromator was used for illumination. The modulation frequency was 8 Hz. The SPV signals were detected with a high impedance buffer and a double phase lock-in amplifier (EG&G 7260 DSP). SPV measurements were performed at photon energies in the spectral range between 0.5 eV and 4.5 eV. For SPV measurements, Mo-coated glass substrates were used.

Optical properties were investigated by measuring transmission and reflection spectra with a Lambda 950 spectrophotometer. The measurements were carried out with an integrating sphere. Absorption spectra were determined by subtracting transmission and reflection from 100%. For optical measurements, glass substrates were used.

### **3. Results and discussion**

#### **3.1 Morphology, composition and crystal phase analysis.**

Figure 1 shows SEM micrographs of the sample surfaces before (a) and after deposition of silver (b-f) (for low magnification SEM micrographs of the same samples, see Supporting Information). Figure 1 (a) shows a top view of an  $\text{In}_2\text{S}_3$  layer deposited on c-Si. The  $\text{In}_2\text{S}_3$  layers were relatively rough with sizes of agglomerates in the order of 50-100 nm. After deposition of silver for 0.5 min (b), the layer became more homogeneous and the originally very small grains could not be distinguished any more. After silver deposition for 4 min, the sample surface became even more homogeneous but small dots with bright contrast and diameters in the order of 10 nm appeared (c). The diameter and the density of these dots increased after silver deposition for 8 min (d). Silver deposition for 16 min (e and f) resulted in a very smooth layer with a thickness of the order of 90 nm (f) covered by particles with bright contrast (e) and a size of about 100-200 nm.

The sample with silver deposited for 16 min has been analyzed by EDX mapping as shown in Figure 2. The intensity of silver signals correlated very well with the appearance of nanoparticles with bright contrast. In contrast, the intensities of the indium and sulfur signals did not correlate with these nanoparticles. Therefore, the nanoparticles consisted of silver and were located on top of the homogeneous  $\text{In}_2\text{S}_3$  precursor layer.

The area covered by the Ag NPs has been extracted by Image J software from SEM images with an area of  $1.50 \times 1.04 \mu\text{m}^2$ . The Image J software was used which makes use of contrast discrimination. The average diameter is obtained from the diameter of each Ag NP. The diameter of each Ag NP is calculated from its coverage area using the equation— $A = \pi(d/2)^2$ , among which A and d are the coverage area and the diameter of the Ag NP, respectively. This calculation presumes a spherical shape of the nanoparticles. The very good and comparable contrast of silver nanoparticles in all the images allowed for precise measurements, the results of them are demonstrated in Figure 3(a).

From the SEM images, Ag NPs were first observed after 4 min of Ag deposition. With increasing the Ag deposition time to 16 min, the coverage and average diameter of Ag NPs were increased from 0.53% and 9.5 nm (4 min sample) to 36.4% and 79 nm (16 min sample), respectively. For the sample with 32 min deposition of Ag, the coverage of Ag NPs increased to 64%, but because many of the Ag NPs are connected, it is hard and pointless to distinguish every particle as well as calculate the average diameter. The numbers of Ag NPs were 76, 204 and 78 on the defined area for Ag deposition for 4, 8 and 16 min, respectively. As a result, Ag NPs can be deposited onto transformed  $\text{In}_2\text{S}_3$  precursor layers whereas the size of Ag NPs can be controlled between ten(s) and hundred(s) of nm by varying the deposition time. This opens the opportunity to incorporate plasmonic Ag NPs into systems with transformed  $\text{In}_2\text{S}_3$  precursor layers. Using the same spray-CVD approach, Ag NPs can also be grown on c-Si substrates. Compared to the physical method used to incorporate Ag plasmonic films in a-

Si:H solar cells [25], the spray-CVD used in this work has the advantages that it allows good control over particle size and density of Ag NPs; furthermore, it is a one step, low temperature process. Disadvantages of spray-CVD for Ag NPs preparation as presented in this work are the requirement of nitrogen as carrier gas for the reaction and so far a limitation to Ag NPs smaller than 100 nm in diameter.

The dependence of the overall molar Ag/In ratio on the deposition time of the silver precursor is presented in Figure 3(b). For a constant deposition rate of silver, the overall molar Ag/In ratio would depend linearly on the deposition time. However, the slope of the dependence of the overall molar Ag/In ratio on the deposition time decreased strongly between 1 and 4 min and between 4 and 8 min. The reduction of the deposition rate follows from the smoothening of the layer due to phase transitions. On the other hand, the slope of the dependence of the overall molar Ag/In ratio on the deposition time increased between 8 and 16 min due to an increase of the surface area by nucleating and growing of Ag NPs. Finally, the slope of the dependence of the overall molar Ag/In ratio on the deposition time decreased between 16 and 32 min due to the onset of forming a compact silver layer.

All the data mentioned above, including coverage of Ag NPs, average of diameter of Ag NPs, density of Ag NPs and silver to indium overall molar ratio are summarized in Table 1.

Obviously, the introduction of silver into  $\text{In}_2\text{S}_3$  precursor layers causes strong changes in the stoichiometry and related phase transitions are expected. Figure 4 gives XRD patterns for an  $\text{In}_2\text{S}_3$  layer and for samples after silver deposition for 0.5, 8, 16 and 32 min. Characteristic peaks of  $\beta\text{-In}_2\text{S}_3$  (JCPDS Files No.: 25-0390),  $\text{AgIn}_5\text{S}_8$  (JCPDS Files No.: 25-1329), orthorhombic  $\text{AgInS}_2$  (JCPDS Files No.: 25-1328), Ag (JCPDS Files No.: 04-0783) and  $\text{Ag}_2\text{S}$  (JCPDS Files No.: 02-0998) are marked in the figure. Only peaks of  $\beta\text{-In}_2\text{S}_3$  were detected for the precursor layer and for the sample after deposition of Ag for 0.5 min. Peaks of both  $\beta\text{-$

$\text{In}_2\text{S}_3$  and  $\text{AgIn}_5\text{S}_8$  were observed for the sample after Ag deposition for 4 min. The peaks of  $\beta\text{-In}_2\text{S}_3$  disappeared and peaks of  $\text{AgIn}_5\text{S}_8$  appeared on the sample after Ag deposition for 8 min. Interestingly, XRD peaks of Ag were not observed on samples after deposition of Ag for 4 and 8 min despite the fact that Ag NPs appeared already in the SEM images. This shows the limited sensitivity of XRD. Peaks of  $\text{AgIn}_5\text{S}_8$ , orthorhombic  $\text{AgInS}_2$ , Ag and  $\text{Ag}_2\text{S}$  were found for the samples after silver deposition for 16 and 32 min. With the analysis of XRD, it can be confirmed that the obtained nanoparticles on top of the layer are indeed pure silver nanoparticles. For the sample after silver deposition for 32 min, the XRD peak of silver increased by 8 times compared to the sample after silver deposition for 16 min.

### 3.2 Surface photovoltage analysis

Transition energies related to phase transitions as confirmed by the XRD measurements could be investigated by a photo-electric method, surface photovoltage (SPV), as it is very sensitive on the changes in electronic states participating in charge separation [26].

The sign of the in-phase SPV signals was positive over the whole spectral range for all samples (not shown). This means that the direction of modulated charge separation did not change. Therefore, the amplitude SPV spectra can be used for the analysis of characteristic transition energies. Figure 5 shows the spectra of the SPV amplitude and of the first derivative for the  $\text{In}_2\text{S}_3$  precursor layer and for the samples after silver deposition for 0.5 and 4 min. The onsets of the SPV spectra shifted to lower photon energy with increasing time of silver deposition. Additionally, shoulders in the increasing part of the SPV spectra could be distinguished, for example, for the sample with a silver deposition time of 4 min. The shoulders appeared as local maxima in the spectra of the first derivative. Characteristic transition energies can be defined by the peak positions in the spectra of the first derivative (energy of derivative peak analysis:  $E_{\text{dpa}}$ ). The values of  $E_{\text{dpa}}$  were found from fitting of the first derivative of the modulated SPV amplitude spectra in the part of increasing signals with a

minimum number of Gaussians. The first derivatives for the samples shown in Figure 5 were fitted with 1, 2 and 3 Gaussians, respectively, whereas exponential tails at the lower photon energies were not taken into account. Figure 6 gives examples for the derivative peak analysis by fitting with two and three Gaussians for the SPV amplitude spectra of the samples after Ag deposition for 0.5 and 4 min, respectively.

The peak positions found by the derivative peak analysis can be compared with the optical band gaps of pure phases. For example, the value of  $E_{\text{dpa}}$  was 2.1 eV for the untreated precursor layer which corresponded well to the band gap of  $\beta\text{-In}_2\text{S}_3$  [26]. However, transitions related to defect states below the band gap can give a value for  $E_{\text{dpa}}$  as well. Therefore, a dependence of the values of  $E_{\text{dpa}}$  on the silver deposition time does not give direct information about phase transitions. One can even state that the dependence of the values of  $E_{\text{dpa}}$  on the silver deposition time gives very sensitively information about the formation of defect bands before phase transitions start.

Figure 7 summarizes the phase analysis (XRD and SEM) and the first derivative peak analysis (SPV) as a function of the silver deposition time. The  $\beta\text{-In}_2\text{S}_3$  layer showed one peak at 2.1 eV corresponding to the band gap of  $\beta\text{-In}_2\text{S}_3$ . Two peaks at 2.2 and 1.96 eV can be identified after Ag deposition for 0.17 min whereas no new phases were observed yet in SEM or XRD. The two peaks shifted to 2.36 and 1.92 eV, respectively, after Ag deposition for 0.5 min. A third peak had to be introduced for the SPV fitting analysis of the 1 min sample. The three peaks were at 2.34, 1.85 and 1.4 eV for the sample after Ag deposition for 1 min. The positive part of the first derivative of the 4 min sample could be fitted with three Gaussians peaked at 1.9, 1.58 and 1.34 eV. The peak at the low energy shifted to 1.17, 1.18 and 1.0 eV for the samples after Ag deposition for 8, 16 and 32 min, respectively, whereas the peak at around 1.6 eV remained practically constant.

The  $\text{AgIn}_5\text{S}_8$  and Ag phases appeared for Ag deposition times between 1 and 4 min from XRD and SEM, respectively, which correlated with the disappearance of the peak at around 2.3 eV and the appearance of the intermediate peak at around 1.6 eV. The appearance of the  $\text{Ag}_2\text{S}$  phase correlated with the shift of the low energy peak towards 1 eV. As remark, the band gap of the  $\text{Ag}_2\text{S}$  phase ranges between 0.9 and 1.1 eV [14, 15]. The peak between 1.8 and 1.9 eV can be related to a defect band which could be converted into the band gap of  $\text{AgIn}_5\text{S}_8$  (between 1.7 and 1.8 eV [27, 28]) and/or of orthorhombic  $\text{AgInS}_2$  (band gap around 1.96 eV [16, 17]). As remark, the peak between 1.8 and 1.9 eV disappeared in the spectrum of the first derivative due to the decrease of the SPV amplitude in this spectral range (change of the charge separation mechanism). In this context, it has to be mentioned that the peak around 1.6 eV is probably not related to the band gap of a given phase but to a defect band.

### 3.3 Optical analysis

Ag NPs can lead to plasmonic absorption enhancement based on different mechanisms, like high-angle scattering, near-field enhancement and coupling into wave-guide modes [4]. Depending on the different mechanisms, the optimum size and density of Ag NPs vary significantly [6, 9, 29, 30]. For testing properties of semiconductor layers, SPV is a powerful tool. However, it is not able to make a clear statement about the optical properties of the Ag NPs from the SPV spectra. Therefore, optical characterization of the layer system with integration of Ag NPs was performed by UV-Vis spectroscopy. To investigate whether there is a plasmonic response of Ag NPs formed on the precursor layer, the absorption property of the  $\text{In}_2\text{S}_3$  precursor layer was compared to the reacted layer with Ag NPs on top. The absorption spectra for the  $\text{In}_2\text{S}_3$  precursor layer and for the layer after deposition of Ag for 16 min are shown in Figure 8. For the absorption spectra of the latter, there is an obvious absorption peak at 380 nm which is related to the absorption peak of Ag NPs [31], and for longer wavelengths, the absorption is higher than for the  $\text{In}_2\text{S}_3$  precursor layer. This shows

clearly that the deposition of Ag NPs onto  $\text{In}_2\text{S}_3$  precursor layer caused an enhanced absorption. For the samples with deposition of Ag for shorter times, before nucleation of Ag nanoparticles, no signature of plasmonic absorption peaks was observed (up to the 8 min sample). For the 32 min sample, the signature of the plasmonic peak remained and broadened. As  $\text{AgInS}_2$  may be used as an absorber material in solar cells with extremely thin absorber, such absorption enhancement would be important for improving the solar energy conversion efficiency in such kind of solar cells. UV-Vis measurements cannot distinguish between (parasitic) absorption in the Ag nanoparticles and beneficial absorption enhancement in the absorber layer. For this purpose electrical measurements on the completed devices will need to be performed.

### 3.4 Scheme of phase transitions during silver deposition onto $\text{In}_2\text{S}_3$ precursor layers

Finally, based on the analysis of SEM, ICP, XRD and SPV results, the following reactions during the deposition of Ag onto an  $\text{In}_2\text{S}_3$  precursor layer were summarized in a scheme which is shown in Figure 9. At the first step of deposition, silver penetrated into the  $\text{In}_2\text{S}_3$  precursor layer and a silver doped  $\text{In}_2\text{S}_3:\text{Ag}$  layer was formed and surface planarization started. During this process, deep defect bands being almost close to transitions related to  $\text{AgIn}_5\text{S}_8$  were developed.

With increasing deposition time of silver, the  $\text{AgIn}_5\text{S}_8$  phase appeared and a composite of  $\text{In}_2\text{S}_3:\text{Ag}$  and  $\text{AgIn}_5\text{S}_8$  started to develop. The nucleation of Ag NPs started on top of saturated  $\text{AgIn}_5\text{S}_8$ . In the following,  $\text{In}_2\text{S}_3:\text{Ag}$  disappeared and a composite of  $\text{AgIn}_5\text{S}_8$  and the orthorhombic phase of  $\text{AgInS}_2$  appeared. The nucleation and the growth of Ag NPs continued and the  $\text{Ag}_2\text{S}$  phase started to form at the interface between Ag NPs and the  $\text{AgIn}_5\text{S}_8$  and/or  $\text{AgInS}_2$ . The formation of the  $\text{Ag}_2\text{S}$  phase could be explained by reaction between Ag NPs and  $\text{AgInS}_2$ .

Nucleated Ag NPs grew larger with increasing deposition time so that agglomeration of neighboring Ag NPs set in. At the last step, neighboring Ag NPs merged with each other and formed irregular islands of silver, i.e. isolated Ag NPs disappeared.

Finally a question which is still under investigation must be pointed out. The formation of binary and ternary Ag compounds is explained by reaction of metallic silver. However, if this is true and not by reaction of  $\text{Ag}^+$  from  $\text{Ag}(\text{hfacac})(\text{PMe}_3)$  before pyrolysis, which is not very likely, Ag must be oxidized from oxidation state 0 to +1, necessarily a redox reaction must take place, i.e. another species must be reduced. But so far, no indication of a reduced species in the films was detected by XRD.

#### **4. Conclusion and outlook**

In this work, phase transitions during the deposition of Ag nanoparticles onto  $\text{In}_2\text{S}_3$  precursor layers were investigated. Using spray chemical vapor deposition, Ag nanoparticles with different sizes and densities were deposited on top of the  $\text{In}_2\text{S}_3$  precursor layers by a simple control of the deposition time. The  $\text{In}_2\text{S}_3$  precursor layers were detected transforming into  $\text{AgIn}_5\text{S}_8$ , orthorhombic  $\text{AgInS}_2$  and  $\text{Ag}_2\text{S}$  phases with increasing the deposition time. After the phase transitions, the layer still shows semiconducting properties, which allows further use as absorber in solar cells. Plasmonic absorption enhancement has been demonstrated for the layer after deposition of Ag for 16 min. The phase transition approach for the deposition of silver nanoparticles on semiconducting layers is promising for the application of plasmonics on solar cells with extremely thin absorber, as it opens the opportunity not only to tune the size or density of Ag NPs but can also help to solve the problem of stable integration of Ag NPs on top of sulfide absorber layers. It is planned to integrate related layer systems with Ag NPs into solar cells with extremely thin absorber and to investigate the plasmonic enhancement of the light trapping and its influence on the solar energy conversion efficiency.

## Acknowledgment

Y. Liu is grateful to the China Scholarship Council (201306630015) for financial support. Dr.

Iver Lauermann is acknowledged for the useful discussions.

## REFERENCES

- [1] A. Polman, *Applied physics. Plasmonics applied*, Science 322 (2008) 868-869.
- [2] R. Zia, J.A. Schuller, A. Chandran, M.L. Brongersma, *Plasmonics: the next chip-scale technology*, Mater. Today 9 (2006) 20-27.
- [3] S. Linic, P. Christopher, D.B. Ingram, *Plasmonic-metal nanostructures for efficient conversion of solar to chemical energy*, Nat. Mater. 10 (2011) 911-921.
- [4] H.A. Atwater, A. Polman, *Plasmonics for improved photovoltaic devices*, Nat. Mater. 9 (2010) 205-213.
- [5] R.A. Pala, J. White, E. Barnard, J. Liu, M.L. Brongersma, *Design of Plasmonic Thin-Film Solar Cells with Broadband Absorption Enhancements*, Adv. Mater. 21 (2009) 3504-3509.
- [6] V.E. Ferry, M.A. Verschuuren, H.B. Li, E. Verhagen, R.J. Walters, R.E. Schropp, H.A. Atwater, A. Polman, *Light trapping in ultrathin plasmonic solar cells*, Opt. Express 18 (2010) A237-A245.
- [7] M. van Lare, F. Lenzmann, M.A. Verschuuren, A. Polman, *Mode coupling by plasmonic surface scatterers in thin-film silicon solar cells*, Appl. Phys. Lett. 101 (2012) 221110.
- [8] V.E. Ferry, M.A. Verschuuren, M.C. Lare, R.E. Schropp, H.A. Atwater, A. Polman, *Optimized spatial correlations for broadband light trapping nanopatterns in high efficiency ultrathin film a-Si:H solar cells*, Nano Lett. 11 (2011) 4239-4245.
- [9] S.-S. Kim, S.-I. Na, J. Jo, D.-Y. Kim, Y.-C. Nah, *Plasmon enhanced performance of organic solar cells using electrodeposited Ag nanoparticles*, Appl. Phys. Lett. 93 (2008) 073307.
- [10] M. Schmid, J. Klaer, R. Klenk, M. Topič, J. Krč, *Stability of plasmonic metal nanoparticles integrated in the back contact of ultra-thin Cu(In,Ga)S<sub>2</sub> solar cells*, Thin Solid Films 527 (2013) 308-313.
- [11] M. Schmid, R. Klenk, M. Lux-Steiner, M. Topič, J. Krč, *Modeling plasmonic scattering combined with thin-film optics*, Nanotechnology 22 (2011) 025204.
- [12] K. Ernst, A. Belaidi, R. Könenkamp, *Solar cell with extremely thin absorber on highly structured substrate*, Semicond. Sci. Technol. 18 (2003) 475-479.
- [13] T. Dittrich, A. Belaidi, A. Ennaoui, *Concepts of inorganic solid-state nanostructured solar cells*, Sol. Energy Mater. Sol. Cells 95 (2011) 1527-1536.
- [14] S.I. Boldish, W.B. White, *Optical band gaps of selected ternary sulfide minerals*, Am. Mineral. 83 (1998) 865-871.
- [15] C. Chen, Y. Xie, G. Ali, S.H. Yoo, S.O. Cho, *Improved conversion efficiency of Ag<sub>2</sub>S quantum dot-sensitized solar cells based on TiO<sub>2</sub> nanotubes with a ZnO recombination barrier layer*, Nanoscale Res. Lett. 6 (2011) 462.
- [16] J.L. Shay, B. Tell, L.M. Schiavone, H.M. Kasper, F. Thiel, *Energy bands of AgInS<sub>2</sub> in the chalcopyrite and orthorhombic structures*, Phys. Rev. B 9 (1974) 1719-1723.
- [17] M.L.A. Aguilera, M. Ortega-López, V.M.S. Resendiz, J.A. Hernández, M.A.G. Trujillo, *Some physical properties of chalcopyrite and orthorhombic AgInS<sub>2</sub> thin films prepared by spray pyrolysis*, Mater. Sci. Eng., B 102 (2003) 380-384.

- [18] M. Ortega-López, O. Vigil-Galán, F. Cruz Gandarilla, O. Solorza-Feria, Preparation of AgInS<sub>2</sub> chalcopyrite thin films by chemical spray pyrolysis, *Mater. Res. Bull.* 38 (2003) 55-61.
- [19] D. Kieven, T. Dittrich, A. Belaidi, J. Tornow, K. Schwarzburg, N. Allsop, M. Lux-Steiner, Effect of internal surface area on the performance of ZnO/In<sub>2</sub>S<sub>3</sub>/CuSCN solar cells with extremely thin absorber, *Appl. Phys. Lett.* 92 (2008) 1033-1036.
- [20] A. Belaidi, T. Dittrich, D. Kieven, J. Tornow, K. Schwarzburg, M. Kunst, N. Allsop, M.C. Lux-Steiner, S. Gavrilov, ZnO-nanorod arrays for solar cells with extremely thin sulfidic absorber, *Sol. Energy Mater. Sol. Cells* 93 (2009) 1033-1036.
- [21] N.A. Allsop, A. Schönmann, A. Belaidi, H.J. Muffler, B. Mertesacker, W. Bohne, E. Strub, J. Röhrich, M.C. Lux-Steiner, C.H. Fischer, Indium sulfide thin films deposited by the spray ion layer gas reaction technique, *Thin Solid Films* 513 (2006) 52-56.
- [22] C.-H. Fischer, N.A. Allsop, S.E. Gledhill, T. Köhler, M. Krüger, R. Sáez-Araoz, Y. Fu, R. Schwieger, J. Richter, P. Wohlfart, P. Bartsch, N. Lichtenberg, M.C. Lux-Steiner, The spray-ILGAR® (ion layer gas reaction) method for the deposition of thin semiconductor layers: Process and applications for thin film solar cells, *Sol. Energy Mater. Sol. Cells* 95 (2011) 1518-1526.
- [23] K.P. Jochum, U. Weis, B. Stoll, D. Kuzmin, Q. Yang, I. Raczek, D.E. Jacob, A. Stracke, K. Birbaum, D.A. Frick, D. Günther, J. Enzweiler, Determination of Reference Values for NIST SRM 610–617 Glasses Following ISO Guidelines, *Geostand. Geoanal. Res.* 35 (2011) 397-429.
- [24] V. Duzhko, V.Y. Timoshenko, F. Koch, T. Dittrich, Photovoltage in nanocrystalline porous TiO<sub>2</sub>, *Phys. Rev. B* 64 (2001) 075204.
- [25] S. Morawiec, M.J. Mendes, S.A. Filonovich, T. Mateus, S. Mirabella, H. Águas, I. Ferreira, F. Simone, E. Fortunato, R. Martins, F. Priolo, I. Crupi, Broadband photocurrent enhancement in a-Si:H solar cells with plasmonic back reflectors, *Opt. Express* 22 (2014) A1059-A1070.
- [26] A. Juma, J. Kavalakkatt, P. Pistor, B. Latzel, K. Schwarzburg, T. Dittrich, Formation of a disorderd hetero-junction by diffusion of Cu<sup>1</sup> from CuSCN into In<sub>2</sub>S<sub>3</sub> layers: A surface photovoltage study, *Phys. Status Solidi A* 209 (2012) 663-668.
- [27] N.M. Gasanly, A. Serpengüzel, A. Aydinli, O. Gürlu, I. Yilmaz, Donor-acceptor pair recombination in AgIn<sub>5</sub>S<sub>8</sub> single crystals, *J. Appl. Phys.* 85 (1999) 3198-3201.
- [28] K.-W. Cheng, C.-M. Huang, G.-T. Pan, W.-S. Chang, T.-C. Lee, T.C.K. Yang, The physical properties and photoresponse of AgIn<sub>5</sub>S<sub>8</sub> polycrystalline film electrodes fabricated by chemical bath deposition, *J. Photochem. Photobiol., A* 190 (2007) 77-87.
- [29] A.A. Yu, W.S. Koh, Resonant and nonresonant plasmonic nanoparticle enhancement for thin-film silicon solar cells, *Nanotechnology* 21 (2010) 235201.
- [30] X. Chen, B. Jia, J.K. Saha, B. Cai, N. Stokes, Q. Qiao, Y. Wang, Z. Shi, M. Gu, Broadband Enhancement in Thin-Film Amorphous Silicon Solar Cells Enabled by Nucleated Silver Nanoparticles, *Nano Lett.* 12 (2012) 2187-2192.
- [31] M.K. Temgire, S.S. Joshi, Optical and structural studies of silver nanoparticles, *Radiat. Phys. Chem.* 71 (2004) 1039-1044.

**Table 1**

<b>Deposition time of Ag (min)</b>	<b>Coverage of Ag NPs (%)</b>	<b>Average diameter of Ag NPs (nm)</b>	<b>Density of Ag NPs</b>	<b>Ag/In molar ratio</b>
0	--	--	0	0.00
0.17	--	--	0	0.12
0.5	--	--	0	0.24
1	--	--	0	0.32
4	0.53	9.5	76	0.68
8	5.2	18	204	0.82
16	36.4	79	78	2.05
32	64	--	--	2.85

**Figure 1**

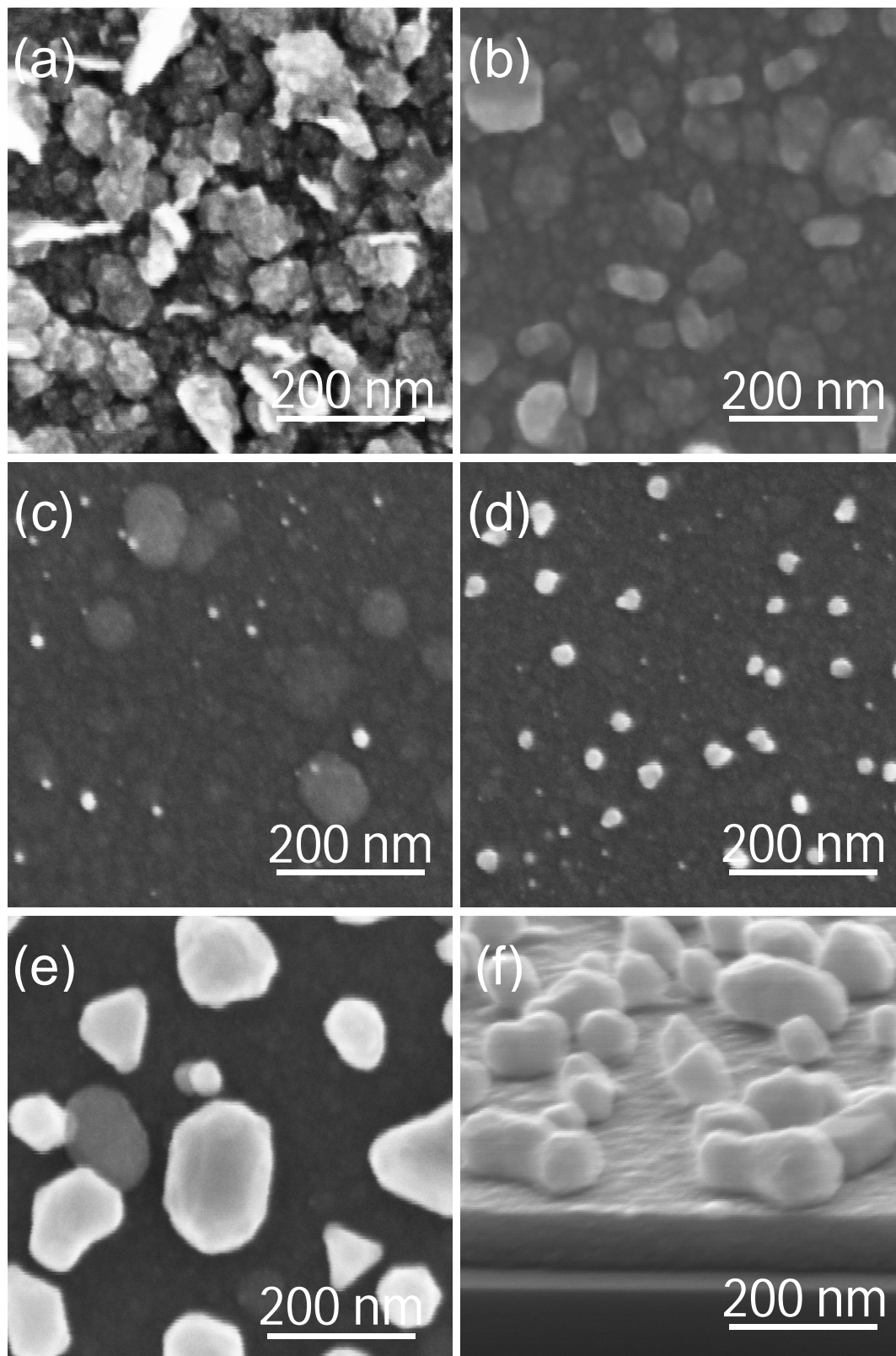


Figure 2

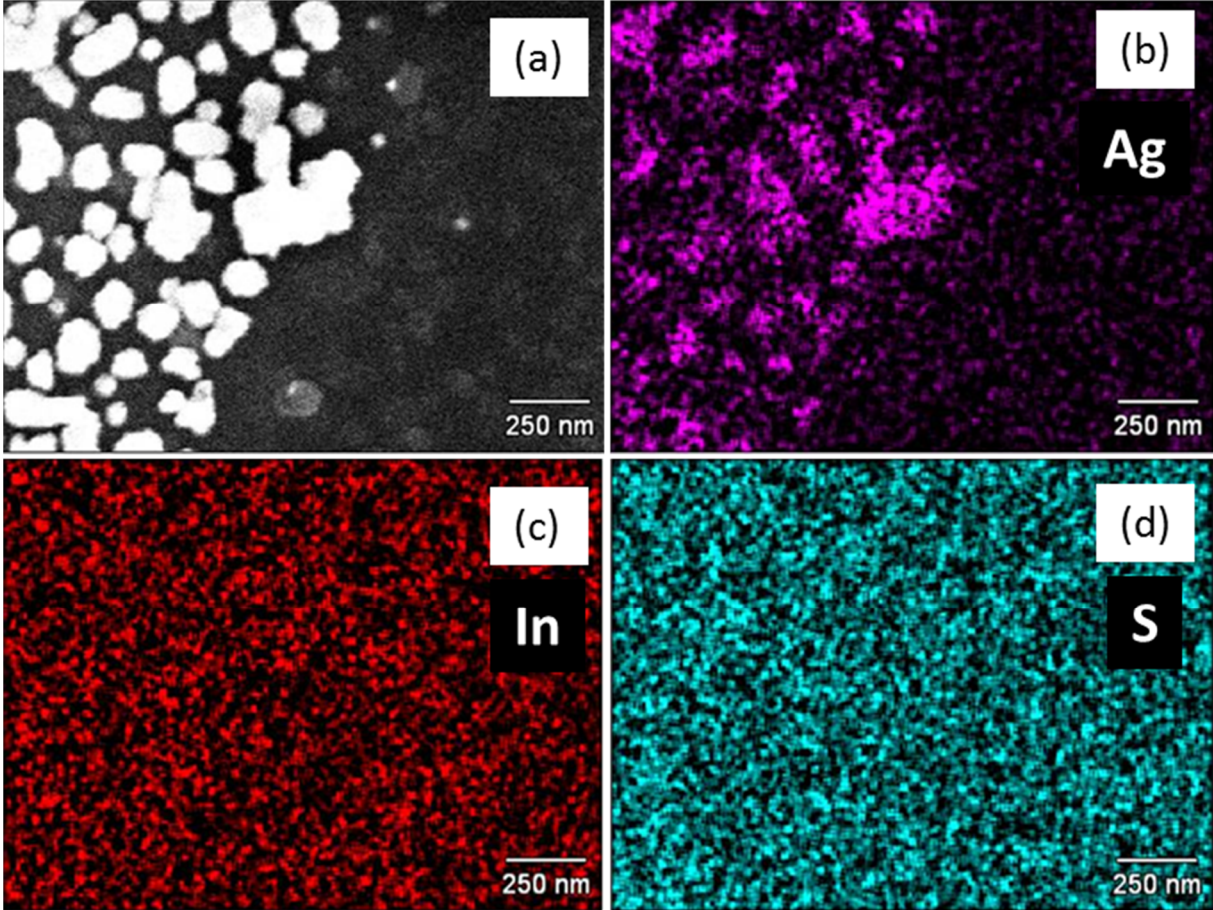


Figure 3

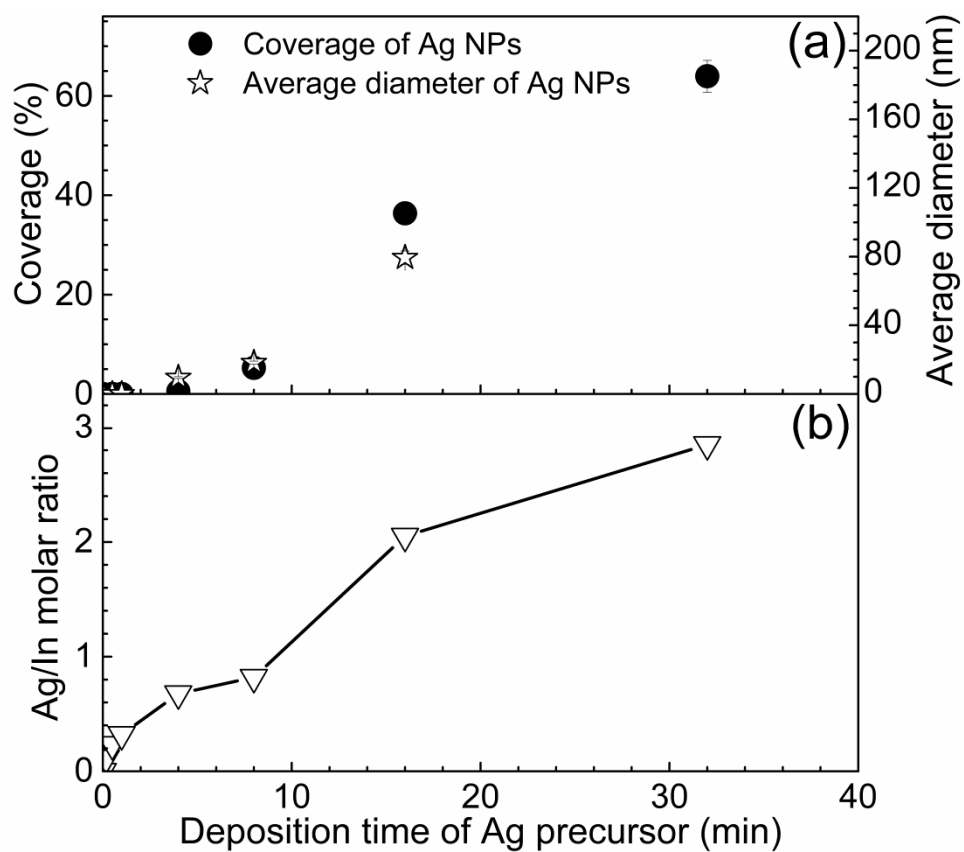


Figure 4

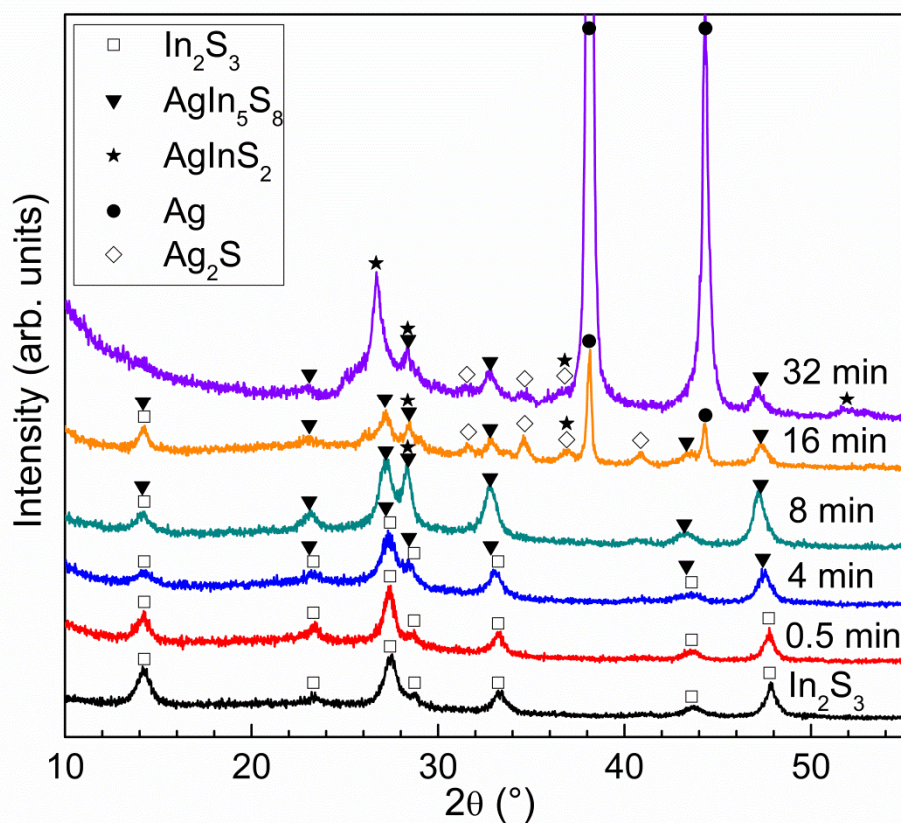


Figure 5

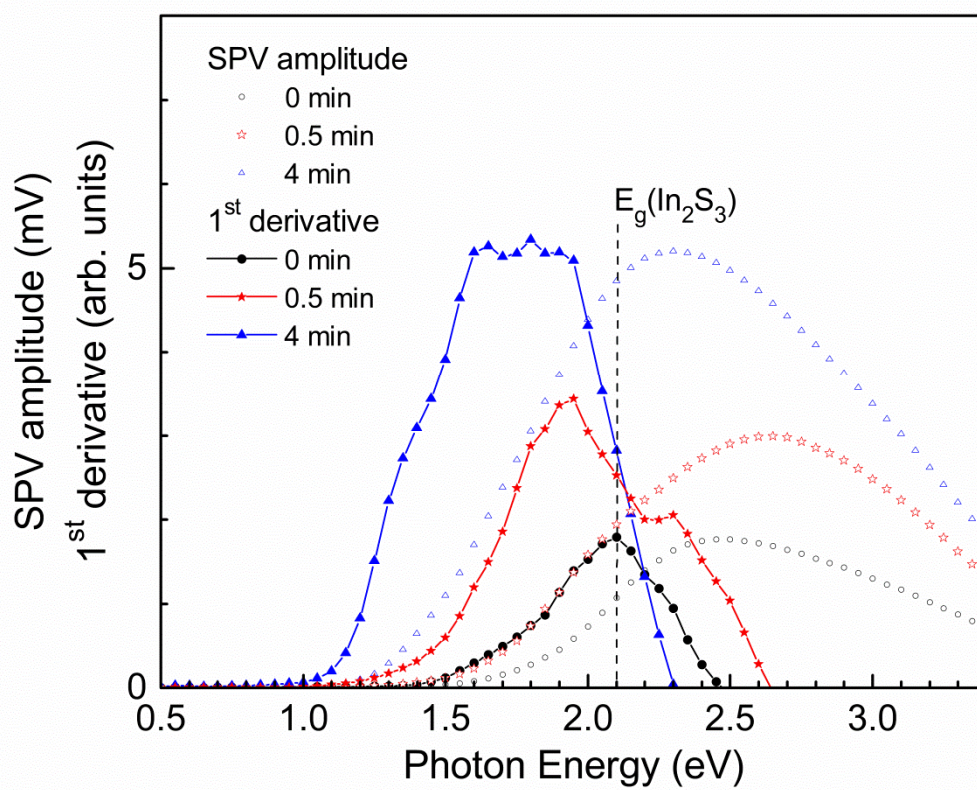


Figure 6

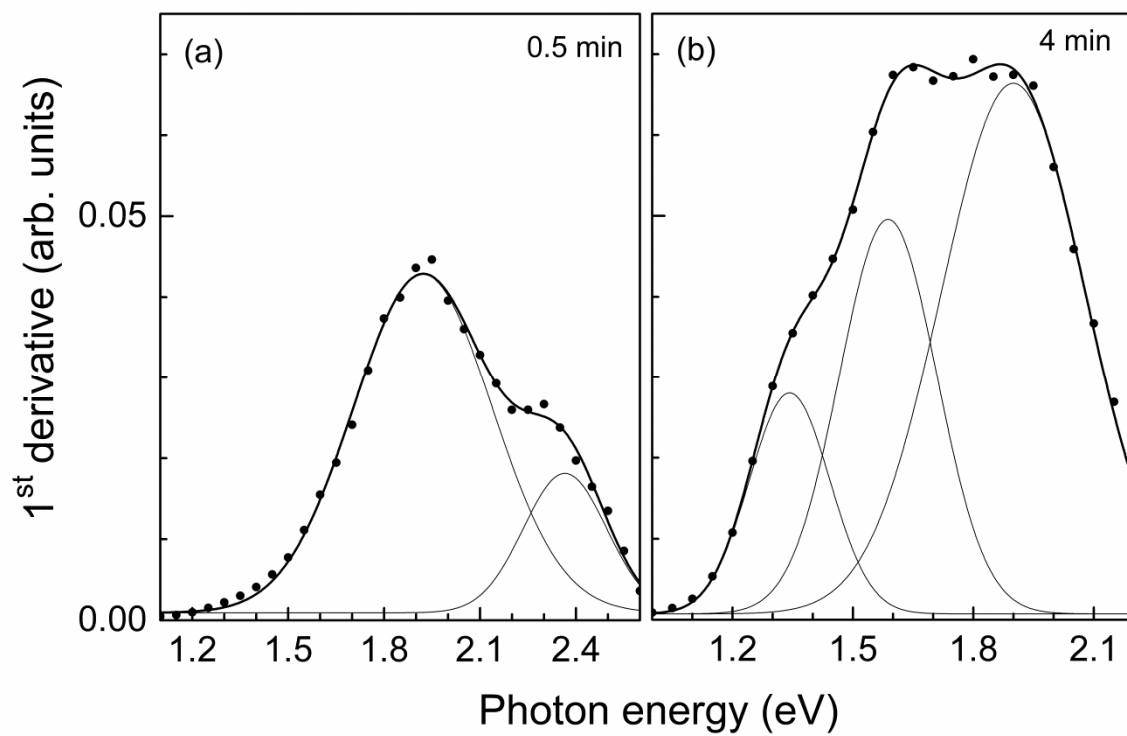


Figure 7

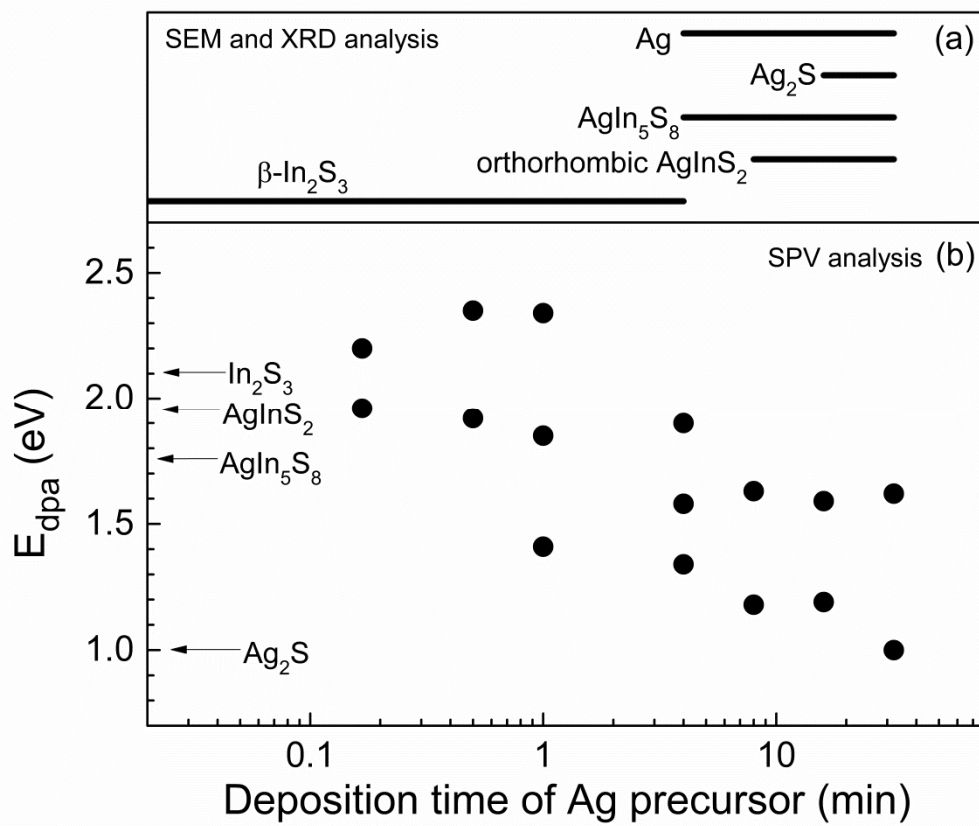


Figure 8

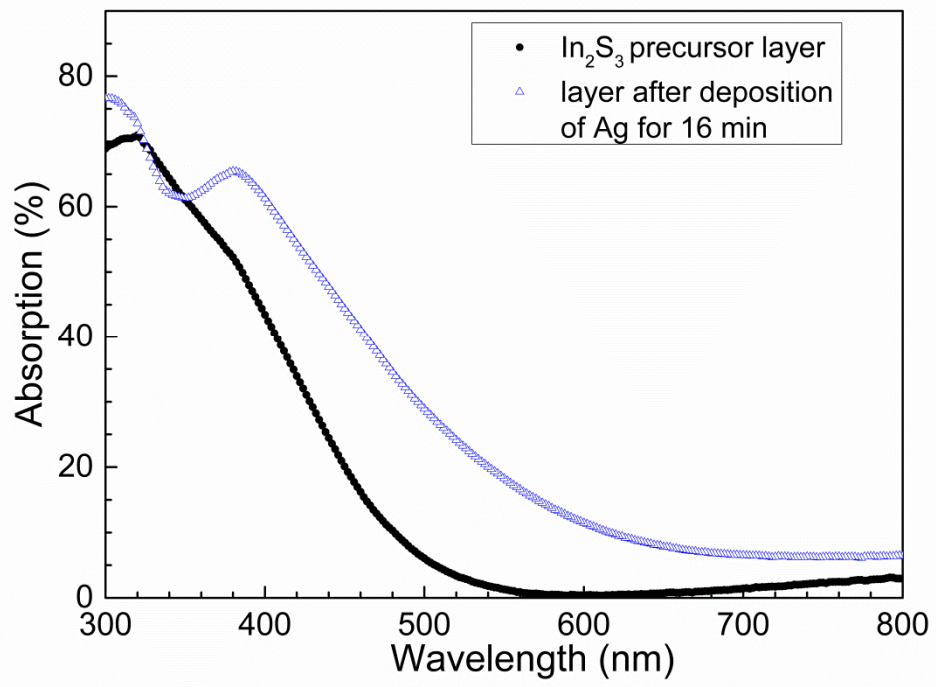
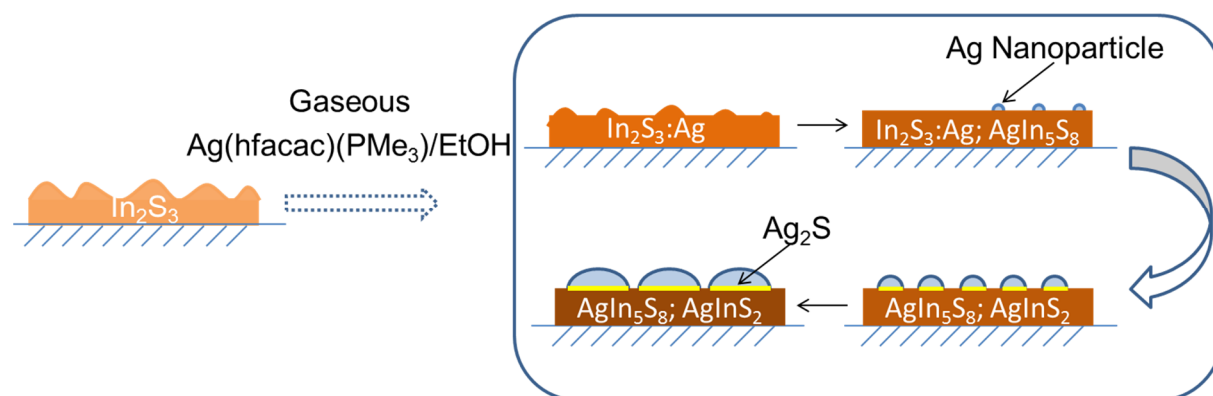


Figure 9



## CAPTIONS

**Figure 1.** Top (a-e) and side (f, tilt angle 30 °) views of c-Si coated with an In<sub>2</sub>S<sub>3</sub> precursor layer after deposition of Ag from an Ag(hfacac)(PMe<sub>3</sub>) source for deposition times of 0 min (a), 0.5 min (b), 4 min (c), 8 min (d) and 16 min (e and f).

**Figure 2.** Top view (a) and maps of Ag, In and S (b-d, respectively) for the c-Si/In<sub>2</sub>S<sub>3</sub> sample after deposition of Ag for 16 min.

**Figure 3.** Dependence of the coverage by Ag nanoparticles (circles) and of the average diameter of Ag nanoparticles (stars) (a) and of the overall molar ratio between silver and indium (b) on the deposition time of Ag.

**Figure 4.** X-ray diffraction spectra of the In<sub>2</sub>S<sub>3</sub> precursor layer deposited on glass before and after deposition of Ag for 0.5, 4, 8, 16 and 32 min. The symbols mark the peaks for β-In<sub>2</sub>S<sub>3</sub> (open squares), AgIn<sub>5</sub>S<sub>8</sub> (filled triangles), orthorhombic AgInS<sub>2</sub> (stars), Ag (circles) and Ag<sub>2</sub>S (open diamonds).

**Figure 5.** Spectra of the SPV amplitudes (open symbols) and of the first derivative for the increasing part of the SPV amplitudes (filled symbols with lines) for the In<sub>2</sub>S<sub>3</sub> precursor layer (circles) and for the layers after deposition of Ag for 0.5 min (stars) and for 4 min (triangles). The dashed lines mark the band gap of β-In<sub>2</sub>S<sub>3</sub>.

**Figure 6.** Fits with Gaussians of the first derivatives of the SPV amplitude spectra in the increasing part for layers after deposition of Ag for 0.5 min (a) and for 4 min (b).

**Figure 7.** Dependence of phases (a) and of the peak positions obtained from the first derivatives of the SPV amplitude spectra in the increasing part (b) on the deposition time of

Ag from a Ag(hfacac)(PMe<sub>3</sub>) source. The arrows mark the band gaps of  $\beta$ -In<sub>2</sub>S<sub>3</sub>, AgIn<sub>5</sub>S<sub>8</sub>, orthorhombic AgInS<sub>2</sub> and Ag<sub>2</sub>S.

**Figure 8.** Absorption spectra for the In<sub>2</sub>S<sub>3</sub> precursor layer (filled circles) and for the layers after deposition of Ag for 16 min (open triangles).

**Figure 9.** Schematic for phase transitions during the deposition of Ag from a Ag(hfacac)(PMe<sub>3</sub>) source on an In<sub>2</sub>S<sub>3</sub> precursor layer.

**Table 1.** Coverage of silver nanoparticles (Ag NPs), average of diameter of Ag NPs, density of Ag NPs (in an area of 1.50×1.04 μm<sup>2</sup>) and silver to indium overall molar ratio dependent on the deposition time of Ag from a Ag(hfacac)(PMe<sub>3</sub>) source.

